High efficiency multilayer coated laminar gratings with high line density for tender X-ray region

Shengyou Wen[1,4,5], Qiushi Huang[1,4,5,6], Andrey Sokolov[2,7], Yeqi Zhuang[1,4,5], Stephanie Lemke[2], Tino Seliger[2], Yue Yu[1,4,5], Igor V. Kozhevnikov[3], Jens Viefhaus[2], Runze Qi[1,4,5], Zhong Zhang[1,4,5] and Zhanshan Wang[1,4,5]

[1]Key Laboratory of Advanced Micro-Structured Materials MOE, Institute of Precision Optical Engineering, School of Physics Science and Engineering, Tongji University, Shanghai 200092, China

[2]Helmholtz-Zentrum Berlin für Materialien und Energie, BESSY-II, Albert-Einstein-Str. 15, 12489 Berlin, Germany

[3]Shubnikov Institute of Crystallography of Federal Scientific Research Centre "Crystallography and Photonics" of the Russian Academy of Sciences, Leninskii pr. 59, Moscow 119333, Russia

[4]Shanghai Professional Technical Service Platform for Full-Spectrum and High-Performance Optical Thin Film Devices and Applications, Tongji University, Shanghai 200092, China

[5]Shanghai Frontiers Science Center of Digital Optics, Tongji University, Shanghai 200092, China

[6]huangqs@tongji.edu.cn

[7]andrey.sokolov@helmholtz-berlin.de

Abstract

High line density multilayer coated laminar gratings (MLLG) were designed, manufactured, and analyzed for operation in photon energy range at 1-5 keV. Theoretical simulation presented in the work are pointing out that a 5000 l/mm MLLG can be employed in high resolution mode at 3 keV with a diffraction efficiency more than 40 times higher than the single layer coated grating. In order to examinate performed simulations, two 3000 l/mm MLLGs were fabricated with different d-spacing optimization: high efficiency MLLG-HE and high resolution MLLG-HR. In the case of MLLG-HE, a maximum efficiency of 54.5% was achieved at 4.4 keV, and for the MLLG-HR, a relatively high efficiency of 23.1% was achieved with a large C_{ff} factor of 4.34 at 4 keV, which can significantly increase the energy resolution of final instrument.

Introduction

The tender X-ray range (1-5 keV) is extremely interesting for spectroscopy-based techniques as it contains many material absorption edges, among them could be mentioned K absorption edges of P, S, Cl, K, Ca, and L absorption edges of some transition metals. Thus, in this energy range one can accurately probe the chemical composition and electronic structure of these elements [1–3], which are of great importance for research into energy chemistry, life science, and environmental science study.

Gratings and crystals are the key dispersion optics in spectrometers and monochromators. Crystal monochromators have high spectral resolution and transmission in hard X-ray range. However small d-spacing in crystals only allows them to operate at near normal incidence in the tender X-ray range, which expose them to very high photon density and thermal load especially for the next generation

diffraction limited ring [4]. Gratings are commonly the main dispersion elements for soft X-rays. However, the efficiency of typical single-layer coated gratings is not higher than few percent even in lowest part of the tender energy range [5].

To fill the tender X-ray range gap, multilayer coated gratings based on combination of multilayer Bragg diffraction and grating diffraction have been developed. Such gratings can achieve more than one order of magnitude higher efficiency compared to single-layer coated gratings and work up to the hard X-ray range under grazing incidence condition [6]. Various types of multilayer gratings are under wide research. The efficiency of ideal multilayer coated blazed grating (MLBG) is rather close to the reflectance of multilayer mirror (MM) and thus exhibits the highest efficiency. Sokolov and Huang et al.[7,8] fabricated the 2400 l/mm Cr/C MLBG and showed a record efficiency of 60% at 3.1 keV and 4.1 keV. Based on this research, a multilayer coated pre-mirror and grating have been installed in the collimated plane grating monochromator at the U41-TXM beamline at BESSY-II synchrotron facility. After extensive commissioning work it was demonstrated that the new setup provides a 100 times more flux at around 2 keV in comparison to single layer coated optics case [1]. Voronov et al.[9,10] developed a dedicated process for fabricating high quality blazed grating and fabricated a 2500 l/m W/B_4C MLBG with a efficiency of 25% at ~1keV. Nevertheless, large size high line density blazed gratings with ultrasmooth surfaces are still difficult to manufacture and not widely available [11,12]. On the other hand, laminar gratings (LG) with periodic profile of rectangular-like groove shapes are easier to fabricate. Polack et al.[13] designed and fabricated a 1200 l/mm Mo/Si MLLG. Over 15% efficiency was measured in the 1.2-1.5 keV range. Chourikani et al.[14] developed a 2400 l/mm B_4C/Mo_2C MLLG for monochromators working in 0.7-3.4 keV range. A peak diffraction efficiency of nearly 27% was measured at 2.2 keV. Due to the L absorption edge of Mo, the efficiency drops sharply above 2.5 keV. The MLLG has also been installed into the DEIMOS beamline monochromator [15].

Besides efficiency, energy resolution is the other critical parameter for monochromator and/or spectrometer. High-resolution spectroscopy techniques such as Resonant Inelastic X-ray Scattering (RIXS) requires diffractive optics with both high efficiency and high resolution. Compared to traditional single-layer coated grating, multilayer grating works at a larger grazing incidence angle which caused lower resolution due to reducing angular dispersion of diffracted beam from the grating. This effect could be easily displayed by commonly used parameter for double elements monochromators: $C_{ff} = \sin(\theta_n) / \sin(\theta_0)$, where θ_0 and θ_n are grazing angles of incident and n^{th} diffraction order beams at the grating [16]. Lower C_{ff} factor leads to lower instrument energy resolution. Increasing the d-spacing of multilayer can reduce the grazing incidence angle and compensate part of the resolution with the same line density grating. Based on this, Feng et al.[17] fabricated an 1800 l/mm Mo/Si MLLG and obtained an efficiency of 25.6% and a C_{ff} factor of 1.79 at 1700 eV. On the other hand, increasing the line density of grating is one of the main methods to improve energy resolution [18,19]. It is especially suitable for multilayer grating since the theoretical efficiency is not significantly affected by line density as for single layer coated gratings

[20]. Voronov et al.[19] fabricated a 10,000 l/mm blazed grating. However, the sawtooth grating profile was considerably smoothed during multilayer coating, causing substantial degradation of MLBG's efficiency. Huang et al. [21] demonstrated a 20,000 l/mm sawtooth multilayer grating fabricated by self-assembled method, while the efficiency was limited by the groove shape. MLLGs with high line density have not been well studied. The exact impact of line density on the theoretical efficiency of MLLG and the optimal relation between multilayer and grating structure for MLLG is still under investigation.

In this paper, the theoretical diffraction characteristics of MLLGs with different line densities and the match of the multilayer d-spacing with grating groove depth for high efficiency were studied in the tender X-ray range. Two high line density MLLGs of 3000 l/mm were fabricated and characterized for high efficiency (HE) and high resolution (HR) purposes, respectively. A maximum efficiency of 54.5% was demonstrated at 4.4 keV with a C_{ff} factor of 3.88, whereas a second MLLG sample showed a C_{ff} factor of 4.34 with an efficiency of 23.1% at 4 keV.

Design and simulation

A schematic diagram of MLLG model is shown in **Error! Reference source not found.**. The bottom is a laminar grating. The grating period is D. Γ is ratio of groove width measured on top to the grating period, and the groove depth is h. ϕ represents the trapezoid angle of the groove profile. In the ideal model, the profile of each layer perfectly reproduces the substrate grating profile, so h and ϕ are constants that do not change with the layer number. The spacer material (S) and absorption material (A) are alternately deposited on the laminar grating, with the periodic thickness d-spacing (d), forming a structure with two-dimensional periods. γ is the ratio of absorption single-layer thickness to d-spacing. The grazing incidence angle (θ_0) of incident light and the diffraction angle (θ_n) of nth order diffraction light are also shown in the figure. In the following simulation, the diffraction order $n = -1$. In the 2-5 keV photon energy range, Cr/C is a good multilayer material combination and was used here [22].

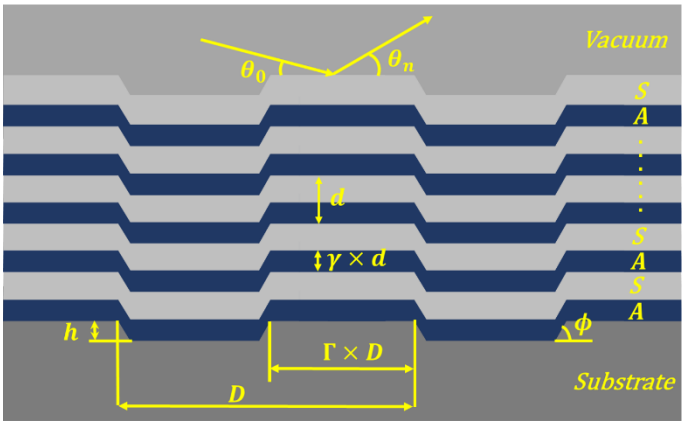

Fig. 1 Schematic diagram of the cross-section of ideal multilayer coated laminar grating

To achieve maximal efficiency at working photon energy, the structure parameters of grating and multilayer should be matched to simultaneously satisfy the grating equation and generalized Bragg

condition[20]. For the high resolution of a grating monochromator/spectrometer, the most critical factor from the grating optics is its dispersion capability and the resulted fix-focus constant C_{ff}.The requirements for efficiency and resolution should be balanced in practical designs.

To study the effect of line density on laminar multilayer grating performance, systematic calculations of the -1st diffraction order efficiency and corresponding C_{ff} factor were carried out for a Cr/C MLLG with various line density (between 1000 l/mm and 5000l/mm) and multilayer d-spacing (from 3 nm to 12nm). Results of simulations at photon energy of 3 keV are shown in Fig.2. Typical profile parameters of laminar gratings manufactured by laser interference lithography were chosen: $\gamma = 0.4, \Gamma = 0.37,\ \phi = 7°$. To see the maximal of reachable efficiency, 200 bilayers were chosen, which were definitely saturated. The groove depth and d-spacing were set to relation $h = 0.5d$, which was considered as one of the optimal conditions providing the maximal diffraction efficiency [20].

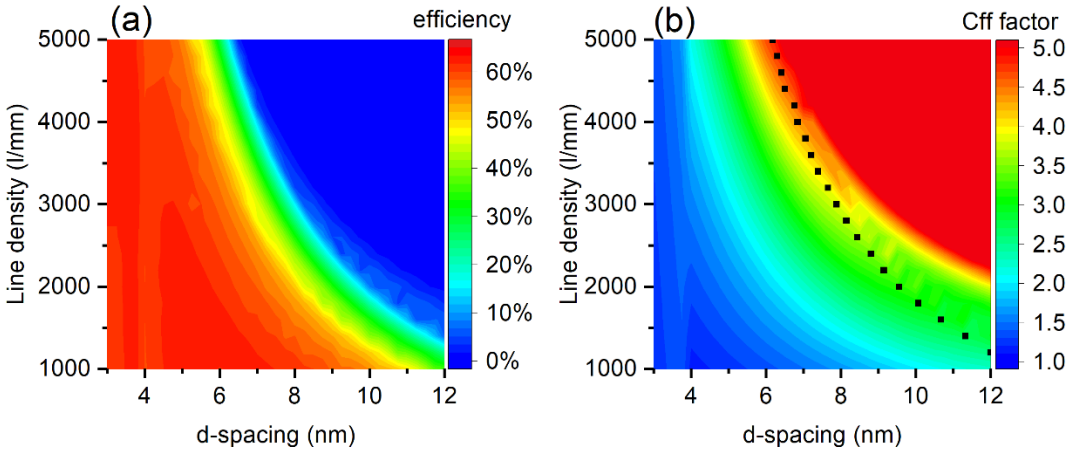

Fig. 2 Calculated diffraction efficiency (a) and C_{ff} factor (b) of MLLGs at 3 keV versus line density and d-spacing, $h = 0.5d$. The black dots represent the MLLGs with efficiency of 20%.

In comparison of these two graphs, one can see a compromise between efficiency and resolution: the areas with higher efficiency correspond to relatively low resolution. The maximal efficiency of 62.5% can be achieved for 1000 l/mm line density with d = 6.5 nm and $C_{ff} = 1.42$ in that case, 61.7% for 3000 l/mm with d = 4.75 nm and $C_{ff} = 1.85$, and 59.8% for 5000 l/mm with d = 4.25 nm and $C_{ff} = 2.34$. With line density increasing the maximum efficiency is barely affected. A sharp drop of efficiency occurs at relatively large d-spacing due to the resonant incident angle approaching the total external reflection (TER) which caused the excitation of 0th order [18]. This threshold of d-spacing gradually decreased with higher line density. At the same time, the C_{ff} factor rises as d-spacing and/or line density increase. Thus, a good balance should be found in MLLG optimization.

Comparing MLLGs with the same efficiency of 20% at different line density (indicated by the black dots in Fig. 2b), the C_{ff} factor is 3.75 for 3000 l/mm MLLG, and that of 5000 l/mm MLLG can reach 4.79 at 3 keV, which is nearly twice that of 1000 l/mm MLLG ($C_{ff} = 2.50$). For the 5000 l/mm Au single layer grating, its efficiency is lower than 0.6% at the same photon energy of 3 keV.

It is about 40~100 times lower than the MLLG. It is evident that high line density MLLG can both improve the resolution and efficiency significantly. As 5000 l/mm grating is currently difficult to fabricate, the line density of 3,000 l/mm was chosen to verify the above analysis in this paper.

The fabrication of a nanometer depth laminar profile for high line density grating is rather challenging and could be achieved with an error of 1.5~2 nm for the h value. Thus, for development of a high quality MLLG, the exact match of grating groove depth and d-spacing and their tolerance is very important. Its effect on efficiency were further studied based on the previous result [20]. The -1st order diffraction efficiency of MLLGs ($3000\,l/mm, \Gamma = 0.37, \phi = 7°, N = 200$) with various d-spacing and groove depth at 3 keV is shown in Fig.3.

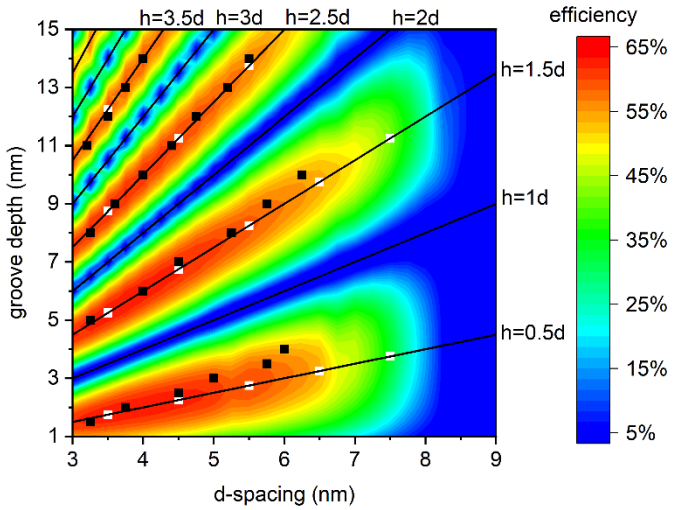

Fig. 3 Calculated -1st diffraction efficiency of MLLGs versus d-spacing and groove depth at 3 keV. The white (black) dots are MLLGs that achieves maximal efficiency at each fixed d-spacing (groove depth).

As shown in Fig.3, the efficiency chart appears radially as the optimum d-spacing is proportional to the groove depth. The efficiency of the structures with $d > 8\,nm$ is extremely low as the incidence angles are close to the TER. The high-efficiency structures are located around several line areas with $h = (k - 0.5) \times d\ (k = 1,2,\dots)$, and low-efficiency structures are around $h = k \times d\ (k = 1,2,\dots)$, as indicated by the black lines. In the overall trend, the maximum efficiency only slightly decreases with k increasing. The structure parameters with different k all can correspond to high efficiency, which is an advantage as it provides a large freedom for MLLG design and fabrication. Note that the width of the radial area narrows as k becomes larger which means a smaller tolerance for the fabrication error. The groove depth also cannot be too large due to the obvious shadowing effect during deposition leading to poor multilayer quality. The white dots marked in Fig.3 correspond to the structures that achieve the maximal efficiency at fixed d-spacing with optimized groove depth, and the results follow exactly the trend of $h = (k - 0.5) \times d$. The black dots represent structures with maximal efficiency at fixed groove depth, which are slightly deviated from the trend and the reason can be explained as follows.

According to the analytic theory [20], the expression of the maximal non-zero order diffraction

efficiency R_n can be described as the following analytic equations:

$$R_n = \frac{1-V}{1+V}, \qquad V = \sqrt{\frac{1-y^2}{1+f^2y^2}}, \qquad y = P_1 \cdot P_2 \cdot P_3$$

$$P_1 = \frac{\sin(\pi j\gamma)}{\pi j(\gamma+g)}, \qquad P_2 = \frac{2\sqrt{\sin\theta_0 \sin\theta_n}}{\sin(\theta_0)+\sin(\theta_n)}, \qquad P_3 = \frac{2}{\pi}\frac{\sin(\pi n\Gamma)}{n}\sin\left(\pi j\frac{h}{d}\right)$$

The parameters f and g are totally determined by the optical constants of multilayer materials. Thus, the larger $|y|$, the higher R_n. The parameter P_1 is constant here because of the same materials, γ and operating energy. P_2 is determined by θ_0 and θ_n which is calculated by the grating equation ($\cos\theta_n = \cos\theta_0 + n\lambda/D$). The effect of h/d on P_3 is sinusoidal and P_3 oscillates faster with smaller d-spacing, resulting in narrower radial area at larger k. Fixing d and optimizing h, P_2 will not change with groove depth. The maximum -1st order efficiency will be achieved when $|P_3|$ is maximal, that is $h/d = k - 0.5$. Fixing h and optimizing d, θ_0 will decrease with d increasing, and P_2 will drop, causing the optimal d to be smaller than $h/(k-0.5)$. This explains the deviation of the two ways of optimization of d and h in Fig 3. Thus, when designing a MLLG for high efficiency, if the groove depth is fixed as obtained from the fabricated grating substrate, the d-spacing needs to be adjusted accordingly. In this case, the optimal relation $h = (k-0.5) \times d$ is not valid and the exact d-spacing requires accurate simulations.

Experiment

According to demonstrated above design and simulations, two MLLGs were fabricated by coating Cr/C multilayers with different d-spacing on a 3000 l/mm laminar grating. The laminar gratings were fabricated using laser interference lithography and ion beam etching at Helmholtz-Zentrum Berlin [23].The grating structure was examined with the atomic force microscopy (AFM) over its whole used aperture before coating multilayer, the average value of groove depth of 3.9 nm, groove width to period ratio Γ of 0.37, and trapezoid angle ϕ of 3.7 degrees. The multilayer parameters were optimized using these measured grating parameters. Fig.4 shows simulated peak efficiency values (a) and C_{ff} factor (b) versus d-spacing for energies from 2 keV to 5 keV. As it seen from Fig.4, the maximum efficiency what can reached is 36.3%-66.5% at 2-5 keV. To achieve maximum efficiency at higher energies one need to apply smaller d-spacing. The C_{ff} factor can be obtained with higher energy and/or larger d-spacing. To obtain maximum efficiency in the energy range of 2-5 keV, $d = 5.7$nm was selected for the MLLG-HE sample. The d-spacing of MLLG-HR sample was selected as 6.7 nm to achieve high resolution and maintain an efficiency of more than 30% in the 2-4 keV energy range. After coating, the d-spacing of the reference MM and MLLG were measured by grazing incidence X-ray reflectometry (XRR) and transmission electron microscopy (TEM) respectively. It was found that final values were almost the same as designed ones.

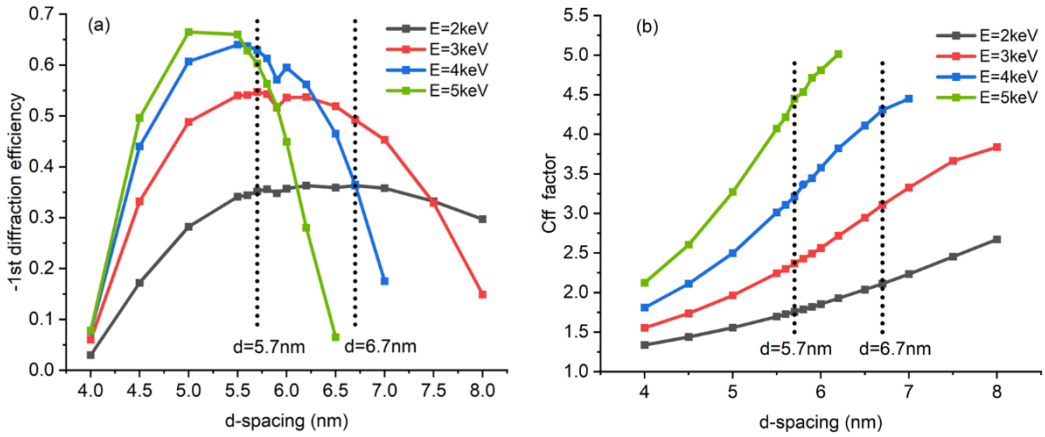

Fig. 4 Calculated -1st diffraction efficiency (a) and C_{ff} (b) versus d-spacing of Cr/C laminar multilayer grating at the energy of 2-5 keV. The black dotted lines show the efficiency and C_{ff} factor at the target d-spacing.

Deposition for Cr/C multilayer coating was performed using a direct-current (DC) magnetron sputtering technique on top of laminar gratings and plane reference mirror samples. High purity Ar was used as sputtering gas under a working pressure of 1.3 mTorr. The thickness ratio (γ) was chosen as 0.4. The bilayer numbers of MLLG-HE and MLLG-HR were 40 and 20, respectively, which were both close to saturated bilayer numbers.

After fabrication, the surface profiles of the reference multilayer mirrors and multilayer gratings were characterized using AFM on a Bruker Dimension Icon system in tapping mode. The scan sizes were $2\ \mu m \times 2\ \mu m$, which consisted of 512×512 pixels. The AFM images of the high efficiency and high resolution MLLG samples are shown in Figs. 5 (b) and (c), respectively. And Fig.5 (d) displays the PSD spectra of the coated gratings and the LG substrate. The major peaks of the PSD spectra after coating remain similar as before with a slight increase at the high spatial frequencies range of $20\sim60\ \mu m^{-1}$. It is indicated that the grating period and groove-to-period ratio of MLLGs are similar to that of LG with a small growth of high frequency roughness after the Cr/C multilayer deposition, as also observed from the AFM images.

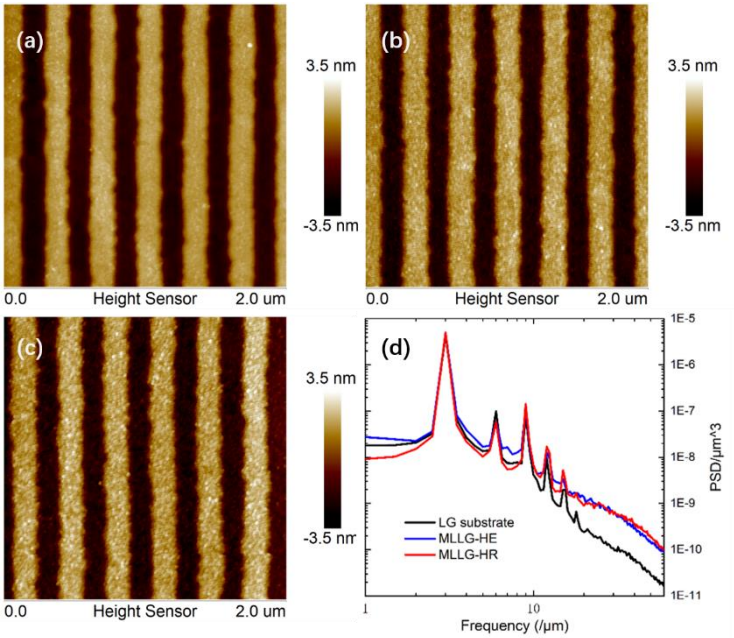

Fig. 5 The AFM surface morphology of (a) laminar grating substrate, (b)MLLG-HE, (c) MLLG-HR, respectively. (d)Comparison of PSD functions.

To analyze the internal multilayer structure on grating, the cross-sectional image of MLLG-HE was obtained by TEM and shown in Fig.6(a). Fig.6(b)~(e) are zoom-in TEM images of side wall areas of the grooves. The dark layers corresponds to Cr and the bright layers to C. From TEM one can see that multilayer structure has good quality with clear and sharp interfaces. To visually display the quality of groove profile replication, the surface/interface profiles of the grating substrate and MLLG-HE after different bilayers deposition were extracted from TEM images and shown in Fig.6(f). It can be seen that, the layer profile well replicated the grating bottom with a slight side shift. The profiles trapezoid angles were almost the same as the substrate one ($\phi_b \approx 4.3°, \phi_c \approx 4.8°, \phi_d \approx 4.75°, \phi_e \approx 4.0°$). The AFM and TEM results consistently prove that there is no obvious smoothing when depositing Cr/C multilayer with a total thickness of about 240 nm on the 3000 l/mm lamellar grating. More obvious smoothening effect should be seen on even higher line density gratings and in the high spatial frequency range [19,24].

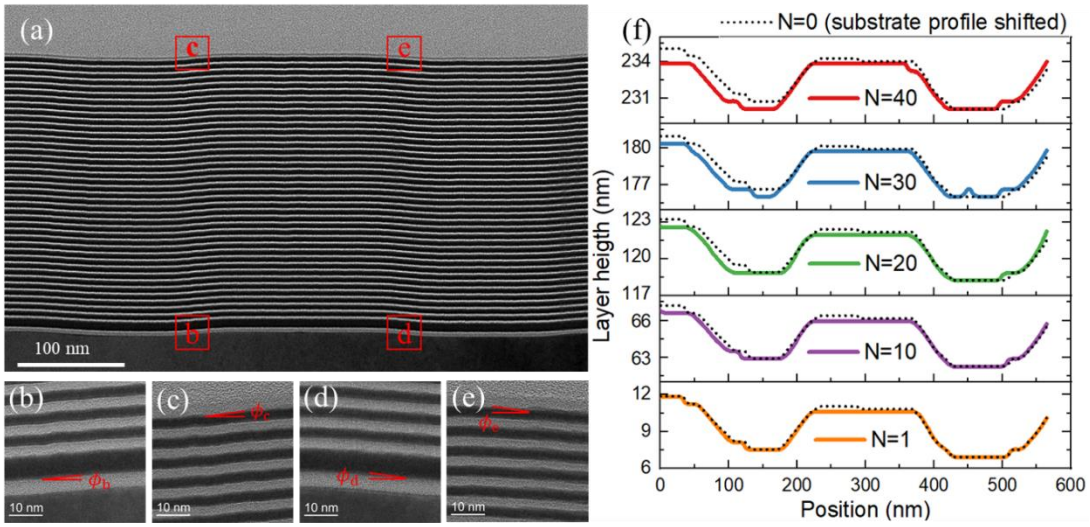

Fig. 6 (a)The whole cross-section TEM images of MLLG-HE. The slope TEM images of MLLG-HE on the left sides of the bottom (b) and top (c) area, and on the right sides of the bottom (d) and top (e) area.
(f) The surface profiles of MLLG-HE substrate and after deposition several bilayers of Cr/C multilayer, obtained from the TEM images. The black dotted curves are the substrate profiles after being shifted.

Tender X-ray measurements

The diffraction efficiency of both MLLG samples and reflectivity of multilayer coating on witness sample were measured in a broad photon energy range from 600 eV up to 5.6 keV. Measurements in XUV energy range were carried out with 11-axis UHV Reflectometer at the Optics Beamline (PM1) [25,26] and the tender x-ray measurements were performed with portable small-Reflectometer [27] at KMC-1 double crystal monochromator beamline [28], which both are at BESSY-II synchrotron radiation facility. The beam spot size on the sample position at optics beamline was $0.36 \times 0.2\ mm^2 (v \times h)$ with vertical divergence of 0.5 mrad. High spectral purity and accurate energy collaboration are provided in the whole beamline energy range and well described in [29]. Sample alignment with respect to the beam were done in all 6-degrees of freedom with in situ UHV tripod system and accuracy better 0.01deg and 0.01mm. Angular scan accuracy of 360 degrees goniometers of sample and detector stages are better than 0.02deg [25]. At the KMC-1 beamline the beam spot size on the sample position was ~0.1 mm vertically with divergence less than 0.2 mrad. The beam intensity stability was supported by MOSTAB control with in-situ feedback system. The measured and ideally calculated efficiencies (assuming perfect multilayer structure) are shown in Fig.7.

The MLLG-HE achieved an efficiency higher than 27.5% throughout the wideband energy range of 2-5 keV. And the maximum efficiency of 54.5% was achieved at 4.4 keV. Relatively small efficiency drop at 3.2 keV does not appear in the calculated curves of reference MM and MLLG-HE, which is caused by the absorption edge of noble sputtering atoms of Ar incorporated in the layers [7]. A 4.0% atomic ratio of Ar was detected mainly in the C layers as measured by energy dispersive X-ray spectroscopy (EDX) obtained with TEM measurements. The difference between the measured and calculated -1st order efficiency at high energies may be due to the measurement

error of the 0th order, and the match of layer thickness with the practical groove profile. For MLLG-HR, its diffraction efficiency is lower than that of MLLG-HE with a maximum efficiency of 38.6% at 3.2 keV. If the interface width and roughness $\sigma = 0.4\,nm$ obtained from XRR fitting and the practical profile of MLLG-HE obtained from TEM are taken into account, the fitting curves of both samples are both close to the measured results which confirmed the theoretical model. Compared to previous research of the high efficiency MLBG[8], the experimental efficiency of MLLG-HE is significantly lower than that at 2-3 KeV range with a efficiency of 10%-15%. This is mainly due to theoretical efficiency differences from the lamellar and blazed grooves of the grating. [20]. Nevertheless, the efficiency of MLLG-HE is only a few percent lower than that of MLBG at around 4keV. Moreover, the fabrication of laminar grating is easier and can bring some advantages in applications.

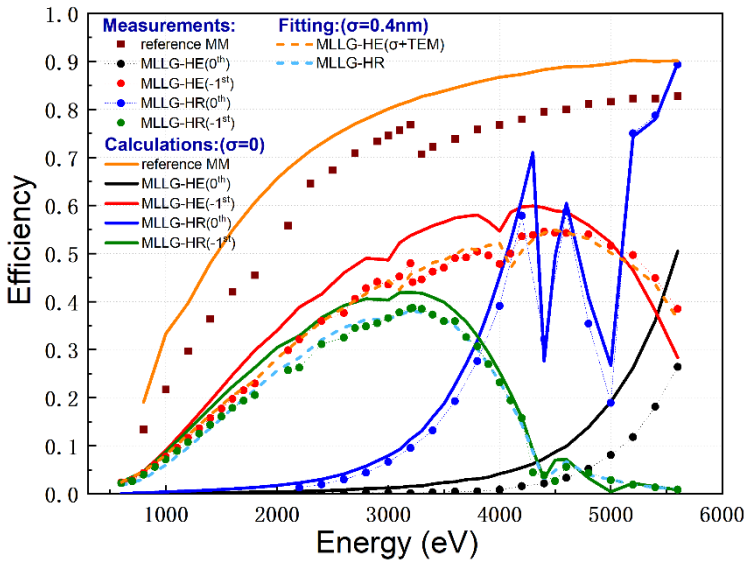

Fig. 7 The measured (points), ideal simulated ($\sigma = 0$, solid curves) 0th and -1st order diffraction efficiency curves of reference MM, MLLG-HE and MLLG-HR. The dotted curves are the -1st order fitting efficiency curves of MLLG-HE ($\sigma = 0.4nm$ and TEM profile) and MLLG-HR ($\sigma = 0.4nm$).

By fixing the grazing incidence angle at the resonance angle (θ_0) of each energy and scanning detector, the angular distribution of -1st order diffraction of two MLLGs was measured at different energy, as shown in Fig. 8(a)(b). Both 0th order and -1st order diffraction peaks were recorded in the measurement, which are marked in the figure. The intensity distribution of diffracted light between 0th and -1st orders is visually displayed on the dispersion plane. The diffraction angles at different working energy can be seen from the figure, which is defined as the angle between incident light and grating plane. Thus, the diffraction angle of the 0th order equals the grazing incidence angle for both 0th and -1st orders. Based on this, the measured C_{ff} factors and the theoretical calculated C_{ff} factors were depicted in Fig.8(c), which are mostly consistent. The small difference of MLLG-HE in high energy might be explained by effects superposition of sample substrate waviness and beam divergence together with residual sample surface misalignment which are relatively increasing their impacts with decreasing of the incident angle. With energy increasing, θ_0 decreases, and C_{ff}

factors increase. MLLG-HE achieved a C_{ff} factor of 3.88 at 4.4 keV with an efficiency of 54.5%. MLLG-HR achieved a C_{ff} factor of 2.76 and maintained an efficiency of 32.5% at 2.6 keV. A high C_{ff} factor of 4.34 was achieved at 4 keV with a practical efficiency of 23.1%.

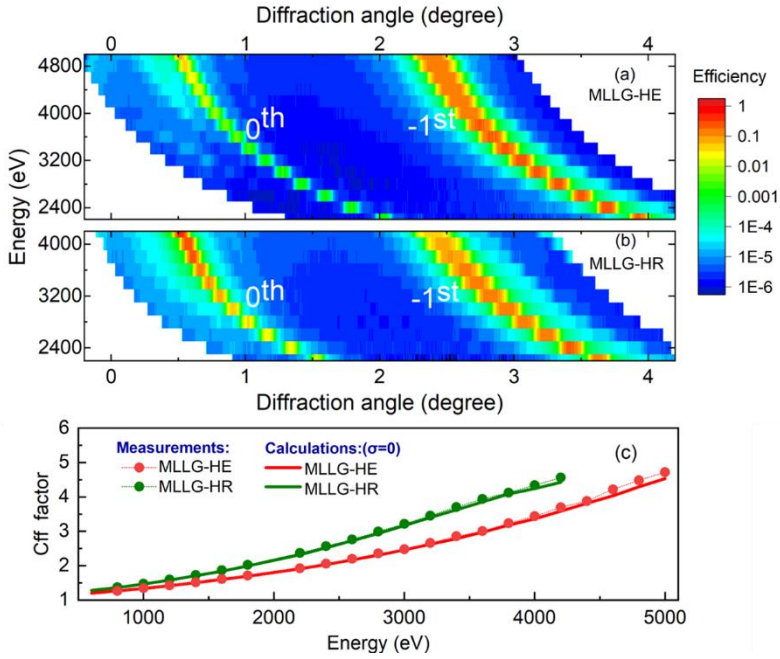

Fig. 8 Detector scans of the MLLG-HE (a) and MLLG-HR(b) measured at different energy. The x-coordinates of 0^{th} order peaks are equal to θ_0, and them of -1^{st} order peak are the corresponding diffraction angles θ_{-1}. (c)The measured (points) and theorical calculated (solid curves) C_{ff} factors of MLLG-HE and MLLG-HR.

Conclusions

The diffraction property of high line density Cr/C MLLGs were theoretically studied and experimentally demonstrated. A higher line density of 3000l/mm to 5000l/mm with optimized d-spacing can significantly enhance the resolution of MLLG with almost the same high efficiency as the conventional 1000l/mm MLLG, in theory. The fabricated MLLG-HE achieved a maximum efficiency of 54.5% at 4.4 keV with a C_{ff} factor of 3.88. The MLLG-HR achieved a C_{ff} factor of 4.34 and maintained an efficiency of 23.1% at 4 keV. Both the efficiency and C_{ff} factor demonstrated are consistent with the theory. It is shown that by combining high line density grating with multilayer, both the advantages of high efficiency and large dispersion can be fully utilized. It will provide a new way for achieving high flux and high resolution monochromator/spectrometer in the tender X-ray region.

Funding

This work was supported by National Natural Science Foundation of China (Nos. 12075170, 12235011).

References

1. S. Werner, P. Guttmann, F. Siewert, A. Sokolov, M. Mast, Q. Huang, Y. Feng, T. Li, F. Senf, R. Follath, Z. Liao, K. Kutukova, J. Zhang, X. Feng, Z. Wang, E. Zschech, and G. Schneider, "Spectromicroscopy of Nanoscale Materials in the Tender X-Ray Regime Enabled by a High Efficient Multilayer-Based Grating Monochromator," Small Methods 2201382 (2022).
2. G. Freychet, E. Gann, L. Thomsen, X. Jiao, and C. R. McNeill, "Resonant Tender X-ray Diffraction for Disclosing the Molecular Packing of Paracrystalline Conjugated Polymer Films," J. Am. Chem. Soc. **143**(3), 1409–1415 (2021).
3. H.-Q. Wang, J. Xu, X. Lin, Y. Li, J. Kang, and J.-C. Zheng, "Determination of the embedded electronic states at nanoscale interface via surface-sensitive photoemission spectroscopy," Light Sci. Appl. **10**(1), 153 (2021).
4. P. Van aerenbergh, C. Detlefs, J. Härtwig, T. A. Lafford, F. Masiello, T. Roth, W. Schmid, P. Wattecamps, L. Zhang, R. Garrett, I. Gentle, K. Nugent, and S. Wilkins, "High Heat Load Diamond Monochromator Project at ESRF," in (2010), pp. 229–232.
5. V. N. Strocov, T. Schmitt, U. Flechsig, T. Schmidt, A. Imhof, Q. Chen, J. Raabe, R. Betemps, D. Zimoch, J. Krempasky, X. Wang, M. Grioni, A. Piazzalunga, and L. Patthey, "High-resolution soft X-ray beamline ADRESS at the Swiss Light Source for resonant inelastic X-ray scattering and angle-resolved photoelectron spectroscopies," J. Synchrotron Radiat. **17**(5), 631–643 (2010).
6. V. A. Chernov, V. I. Erofeev, N. I. Chkhalo, N. V. Kovalenko, and S. V. Mytnichenko, "X-ray performance of multilayer gratings: recent advances at SSRC," Nucl. Instrum. Methods Phys. Res. Sect. Accel. Spectrometers Detect. Assoc. Equip. **405**(2–3), 310–318 (1998).
7. F. Senf, F. Bijkerk, F. Eggenstein, G. Gwalt, Q. Huang, R. Kruijs, O. Kutz, S. Lemke, E. Louis, M. Mertin, I. Packe, I. Rudolph, F. Schäfers, F. Siewert, A. Sokolov, J. M. Sturm, Ch. Waberski, Z. Wang, J. Wolf, T. Zeschke, and A. Erko, "Highly efficient blazed grating with multilayer coating for tender X-ray energies," Opt. Express **24**(12), 13220 (2016).
8. A. Sokolov, Q. Huang, F. Senf, J. Feng, S. Lemke, S. Alimov, J. Knedel, T. Zeschke, O. Kutz, T. Seliger, G. Gwalt, F. Schäfers, F. Siewert, I. V. Kozhevnikov, R. Qi, Z. Zhang, W. Li, and Z. Wang, "Optimized highly efficient multilayer-coated blazed gratings for the tender X-ray region," Opt. Express **27**(12), 16833 (2019).
9. D. L. Voronov, E. M. Gullikson, F. Salmassi, T. Warwick, and H. A. Padmore, "Enhancement of diffraction efficiency via higher-order operation of a multilayer blazed grating," Opt. Lett. **39**(11), 3157 (2014).
10. D. L. Voronov, F. Salmassi, J. Meyer-Ilse, E. M. Gullikson, T. Warwick, and H. A. Padmore, "Refraction effects in soft x-ray multilayer blazed gratings," Opt. Express **24**(11), 11334 (2016).
11. S. Park, D. L. Voronov, and H. Padmore, "Development of low blaze angle gratings for ALS-U," in *Advances in X-Ray/EUV Optics and Components XV*, C. Morawe, A. M. Khounsary, and S. Goto, eds. (SPIE, 2020), p. 7.
12. D. L. Voronov, H. A. Padmore, and P. Lum, "Full size x-ray grating fabrication using large area nanoimprint," in *Advances in X-Ray/EUV Optics and Components XII*, C. Morawe, A. M. Khounsary, and S. Goto, eds. (SPIE, 2017), p. 6.
13. F. Polack, B. Lagarde, M. Idir, A. L. Cloup, E. Jourdain, M. Roulliay, F. Delmotte, J. Gautier, and M.-F. Ravet-Krill, "Alternate Multilayer Gratings with Enhanced Diffraction Efficiency in the 500–5000 eV Energy Domain," in *AIP Conference Proceedings* (AIP, 2007), **879**, pp. 489–492.

14. F. Choueikani, B. Lagarde, F. Delmotte, M. Krumrey, F. Bridou, M. Thomasset, E. Meltchakov, and F. Polack, "High-efficiency B_4C/Mo_2C alternate multilayer grating for monochromators in the photon energy range from 07 to 34 keV," Opt. Lett. **39**(7), 2141 (2014).
15. P. Ohresser, E. Otero, F. Choueikani, K. Chen, S. Stanescu, F. Deschamps, T. Moreno, F. Polack, B. Lagarde, J.-P. Daguerre, F. Marteau, F. Scheurer, L. Joly, J.-P. Kappler, B. Muller, O. Bunau, and Ph. Sainctavit, "DEIMOS: A beamline dedicated to dichroism measurements in the 350–2500 eV energy range," Rev. Sci. Instrum. **85**(1), 013106 (2014).
16. R. Follath and F. Senf, "New plane-grating monochromators for third generation synchrotron radiation light sources," Nucl. Instrum. Methods Phys. Res. Sect. Accel. Spectrometers Detect. Assoc. Equip. **390**(3), 388–394 (1997).
17. Y. Feng, Q. Huang, Y. Zhuang, A. Sokolov, S. Lemke, R. Qi, Z. Zhang, and Z. Wang, "Mo/Si lamellar multilayer gratings with high efficiency and enhanced resolution for the x-ray region of 1000–1700eV," Opt. Express **29**(9), 13416 (2021).
18. Q. Huang, I. V. Kozhevnikov, A. Sokolov, Y. Zhuang, T. Li, J. Feng, F. Siewert, J. Viefhaus, Z. Zhang, and Z. Wang, "Theoretical analysis and optimization of highly efficient multilayer-coated blazed gratings with high fix-focus constant for the tender X-ray region," Opt. Express **28**(2), 821 (2020).
19. D. L. Voronov, E. H. Anderson, R. Cambie, S. Cabrini, S. D. Dhuey, L. I. Goray, E. M. Gullikson, F. Salmassi, T. Warwick, V. V. Yashchuk, and H. A. Padmore, "A 10,000 groove/mm multilayer coated grating for EUV spectroscopy," Opt. Express **19**(7), 6320 (2011).
20. X. Yang, I. V. Kozhevnikov, Q. Huang, H. Wang, M. Hand, K. Sawhney, and Z. Wang, "Analytic theory of alternate multilayer gratings operating in single-order regime," Opt. Express **25**(14), 15987 (2017).
21. Q. Huang, V. Medvedev, R. van de Kruijs, A. Yakshin, E. Louis, and F. Bijkerk, "Spectral tailoring of nanoscale EUV and soft x-ray multilayer optics," Appl. Phys. Rev. **4**(1), 011104 (2017).
22. H. Jiang, A. Michette, S. Pfauntsch, Z. Wang, J. Zhu, and D. Li, "Determination of the evolution of layer thickness errors and interfacial imperfections in ultrathin sputtered Cr/C multilayers using high-resolution transmission electron microscopy," Opt. Express **19**(12), 11815 (2011).
23. F. Siewert, B. Löchel, J. Buchheim, F. Eggenstein, A. Firsov, G. Gwalt, O. Kutz, St. Lemke, B. Nelles, I. Rudolph, F. Schäfers, T. Seliger, F. Senf, A. Sokolov, Ch. Waberski, J. Wolf, T. Zeschke, I. Zizak, R. Follath, T. Arnold, F. Frost, F. Pietag, and A. Erko, "Gratings for synchrotron and FEL beamlines: a project for the manufacture of ultra-precise gratings at Helmholtz Zentrum Berlin," J. Synchrotron Radiat. **25**(1), 91–99 (2018).
24. Q. Huang, Q. jia, J. Feng, H. Huang, X. Yang, J. Grenzer, K. Huang, S. Zhang, J. Lin, H. Zhou, T. You, W. Yu, S. Facsko, P. Jonnard, M. Wu, A. Giglia, Z. Zhang, Z. Liu, Z. Wang, X. Wang, and X. Ou, "Realization of wafer-scale nanogratings with sub-50 nm period through vacancy epitaxy," Nat. Commun. **10**(1), 2437 (2019).
25. F. Eggenstein, P. Bischoff, A. Gaupp, F. Senf, A. Sokolov, T. Zeschke, and F. Schäfers, "A reflectometer for at-wavelength characterization of XUV-reflection gratings," in L. Assoufid, H. Ohashi, and A. K. Asundi, eds. (2014), p. 920607.
26. A. Sokolov, P. Bischoff, F. Eggenstein, A. Erko, A. Gaupp, S. Künstner, M. Mast, J.-S. Schmidt, F. Senf, F. Siewert, Th. Zeschke, and F. Schäfers, "At-wavelength metrology facility for soft X-ray reflection optics," Rev. Sci. Instrum. **87**(5), 052005 (2016).

27. F. Schaefers, S. A. Yulin, T. Feigl, and N. Kaiser, "At-wavelength metrology on Sc-based multilayers for the UV and water window," in A. Duparre and B. Singh, eds. (2003), p. 138.
28. F. Schäfers, "The crystal monochromator beamline KMC-1 at BESSY II," J. Large-Scale Res. Facil. JLSRF **2**, A96 (2016).
29. A. Sokolov, M. G. Sertsu, A. Gaupp, M. Lüttecke, and F. Schäfers, "Efficient high-order suppression system for a metrology beamline," J. Synchrotron Radiat. **25**(1), 100–107 (2018).